Olivine reactivity with CO_2 and H_2O on a microscale: Implications for carbon sequestration

J. Olsson[1*], N. Bovet[1], E. Makovicky[2], K. Bechgaard[1], Z. Balogh[1] and S.L.S. Stipp[1]

[1] Nano-Science Center, Department of Chemistry, University of Copenhagen, Universitetsparken 5, DK-2100 København Ø, Denmark; jolsson@nano.ku.dk; bovet@nano.ku.dk; klbe@kiku.dk; zb@nano.ku.dk; stipp@nano.ku.dk

[2] Department of Geography and Geology, University of Copenhagen. Øster Voldgade 10, DK-1350 Copenhagen K, Denmark; emilm@geo.ku.dk

* corresponding author: jolsson@nano.ku.dk (J. Olsson)

Submitted to *Geochimica et Cosmochimica Acta*

21 March 2011

Revised manuscript

23 September 2011

Abstract

The silicate mineral olivine, $(Mg,Fe)_2SiO_4$, reacts exothermally with CO_2 and forms secondary minerals, including carbonates. Therefore olivine reaction is a promising process for carbon sequestration, to convert carbon dioxide from the atmosphere to mineral form. The purpose of this study was: 1) to explore the composition, structure and reactivity of olivine surfaces during exposure to air and to water at ambient conditions, 2) to investigate the effect of elevated CO_2 pressure and temperature, and 3) to identify the secondary minerals.

Olivine surfaces have been examined with atomic force microscopy (AFM), scanning electron microscopy (SEM) and X-ray photoelectron spectroscopy (XPS), before and after reaction with CO_2. Experiments were carried out in pure water equilibrated with CO_2 at total pressures up to 80 bars, at temperatures 25 °C and 120 °C and both in the absence and presence of oxygen. New formation products appeared on the olivine surface as a homogeneous layer of bumps, less than 100 nm in diameter, within hours of exposure to air. Olivine crystals, exposed to water, dissolved and secondary minerals formed within days. Colonies of bacteria populated olivine surfaces on samples stored in water for more than 4 days at room temperature. Loosely attached material formed on olivine surfaces and could easily be scraped away with the AFM tip. A red precipitate formed when crystals where reacted at increased temperatures and CO_2 partial pressures for less than 4 days. The new phases were identified as goethite, hematite, silica and carbonate minerals. Olivine surfaces oxidise and iron oxides form even when oxygen is absent, suggesting hydrolysis, where water is converted to hydrogen and oxygen.

Key Words

Carbon dioxide sequestration, forsterite, surface-chemistry, basalt, olivine oxidation, passivation layer, olivine dissolution, ultramafic, CCS, forsterite dissolution

1. INTRODUCTION

The world faces a huge challenge: to decrease carbon dioxide emissions while maintaining a reasonable rate of economic growth. Even if non-CO_2 emitting energy forms could be adopted immediately, there would still be a need to sequester the carbon that has already entered the atmosphere, to get back to preindustrial levels of CO_2 and ocean pH. One promising way is to convert CO_2 to carbonate minerals. Silicate minerals, such as olivine, pyroxene and plagioclase, can react with carbon dioxide and form other phases, including carbonate minerals. Advantages of mineralization as a carbon capture and storage (CCS) technology are: (1) Long time stability; the solidified CO_2 is immobilised on a geological time scale (Lackner et al., 1995). (2) Vast capacity; world-wide; there is abundant sequestration material available to bind the CO_2 (Goldberg et al., 2001; Goldberg et al., 2008; Kelemen and Matter, 2008; Oelkers et al., 2008). (3) Carbonate mineral formation is energetically favourable; the thermodynamic driving force promotes these reactions (negative $\Delta G°r$) (Lackner et al., 1995). Unfortunately, at standard temperature and atmospheric CO_2 pressure, the reactions are slow, making mineral carbonation economically unfavourable as a step in industrial fuel cycles (Lackner et al., 1995). However, with decreased pH, such as with higher CO_2 partial pressures, or higher temperatures, such as is found in geothermal areas, reaction rate

increases and the process becomes attractive (McGrail et al., 2006; Oelkers et al., 2008; Matter and Kelemen, 2009; Schaef et al., 2009; Gislason et al., 2010).

Vast amounts of mafic rock, e.g. basalt, dolerite and gabbro, can be found worldwide and these are known to act as natural carbon sinks during weathering, the process where rocks are converted to soil (Brady and Gíslason, 1997; Gaillardet et al., 1999; Kump et al., 2000; Schopka et al., 2011). The option of storing CO_2 permanently in basaltic rock has lately received a lot of attention and the first pilot projects for CO_2 injection into basaltic rock have already been initiated (McGrail et al., 2006; Matter et al., 2007; Alfredsson et al., 2008; Prasad et al., 2009; Gislason et al., 2010). To date, very little is known about the reactions at the basalt rock/CO_2/water interfaces. Therefore, experimental investigations using nanoscale techniques, such as atomic force microscopy (AFM), scanning electron microscopy (SEM) and X-ray photoelectron spectroscopy (XPS), can contribute new insight for helping us develop and improve mineral carbonation technologies for the future.

The pathway for mineral sequestration in basaltic rocks follows two main steps. First, cations must be liberated from the crystal structure of an appropriate silicate mineral and next, the liberated cations must combine with carbon dioxide in aqueous solution where pH is high enough to stabilize the CO_3^{2-} species. Olivine, $(Mg,Fe)_2SiO_4$, forms a complete solid solution series between the Mg end member, forsterite and the Fe end member, fayalite. Both cations form carbonate minerals, magnesite, $MgCO_3$, and siderite, $FeCO_3$. Olivine is a good candidate for CO_2 sequestration because: (1) it is present in basalt, which contributes 8% of the continental crust and most of the oceanic crust; (2) it is a nesosilicate, the silicate group with the lowest ratio of Si:cations, thus the highest rate of

dissolution and the highest capacity for carbon capture; (3) olivine does not contain aluminium, which tends to form clays, thus removing some of the cations that could form carbonate minerals; and (4) mafic and ultramafic rocks are basic, contributing neutralizing capacity for the protons produced when CO_2 reacts with H_2O to form H_2CO_3, thus allowing mineral carbonation to proceed further than would occur during weathering of felsic rocks, such as granite or andesite.

Many experimental studies have been made over the years to describe the dissolution process for olivine as a function of temperature and pH (Wogelius and Walther, 1991; Pokrovsky and Schott, 2000a; Pokrovsky and Schott, 2000b; Rosso and Rimstidt, 2000; Oelkers, 2001; Chen et al., 2006; Hänchen et al., 2006; Wimpenny et al., 2010). It is known that olivine dissolution proceeds faster in acidic than in alkaline solutions and that the dissolution rate is controlled by precursors complexes formed on the mineral surface (Wogelius and Walther, 1991; Pokrovsky and Schott, 2000b; Oelkers, 2001; Hänchen et al., 2006; Schott et al., 2009; Morrow et al., 2010). It is generally accepted that acidic dissolution of forsterite proceeds as Mg^{2+} surface atoms are exchanged for protons. Mg^{2+} is then leached to the solution, leaving a silica rich surface layer. Based on stoichiometric forsterite titration studies, Pokrovsky and Schott proposed that the silica polymerizes and forms a magnesium depleted layer several unit cells thick (< 20 Å) (Pokrovsky and Schott, 2000a; Pokrovsky and Schott, 2000b). A simplified representation of this polymerization reaction can be written as:

$$> SiOH + HOSi < \leftrightarrow > SiOSi < + H_2O, \qquad (1)$$

where > represents surface sites, and where >SiOH sites are likely to be the rate-controlling precursor complexes (Oelkers, 2001). The polymerization process allows protons to penetrate deeper into the olivine bulk, promoting continued dissolution. This is in agreement with a recent ab initio modelling study by Morrow and colleagues confirming the rapid release of Mg^{2+} and polymerization of a Si-rich layer (Morrow et al., 2010).

Other researchers have suggested that the formation of a surface layer, a passivating layer, decreases the rate of dissolution (Grandstaff, 1978; Béarat et al., 2006; Andreani et al., 2009; Garcia et al., 2010; King et al., 2010; Daval et al., 2011). It is also possible that the secondary mineral layer exfoliates when a critical thickness is reached (Jarvis et al., 2009). Béarat et al. (Béarat et al., 2006) presented transmission electron microscopy (TEM) results showing an olivine surface with a 50 nm thick silica layer that formed at high temperatures and CO_2 partial pressures. Thin passivating layers on acid treated olivines have also been observed with XPS (Seyama et al., 1996; Pokrovsky and Schott, 2000a).

The acidic dissolution of olivine can be written as:

$$(Mg,Fe)_2SiO_4 + 4H^+ \rightarrow 2(Mg^{2+},Fe^{2+}) + H_4SiO_4. \qquad (2)$$

As olivine dissolves and silica is produced, protons are consumed, leading to an increase in pH. At conditions far from equilibrium, the dissolution rate for forsterite is independent of the Mg and Si concentrations in solution (Oelkers, 2001). In an experimental study, the forsterite dissolution rate (*r*) was deduced at temperatures ranging

from 90 to150 °C and pH ranging from 2 to 8.5, consistent with the Arrhenius equation (Hänchen et al., 2006):

$$r = Aa_{H^+}^{n} exp\left(\frac{-E_A}{RT}\right), \qquad (3)$$

where A = 0.0854 (+0.67 to -0.076), n = 0.46 ± 0.03 and a_{H+} represents the proton activity; E_a, the activation energy, has a value of 52.9 ± 6.9 kJ/mol, R is the gas constant and T represents the absolute temperature. The uncertainty in A is a function of pH. The experiments were carried out in a carbon dioxide atmosphere at pressures between 15 and 180 bars. In the presence of CO_2, under acidic conditions (pH≤5), at 120 °C, the dissolution rates were double those without CO_2 at the same pH.

Few research labs have succeeded in forming substantial amounts of magnesite (Giammar et al., 2005; Gerdemann et al., 2007; Hänchen et al., 2008). Carbonation of 80% of the reacted olivine after 6 hours was reported at the optimum conditions (Gerdemann et al., 2007). The experiments were made at 185 °C with 150 bars of CO_2 in solutions of 0.64 M $NaHCO_3$ and 1 M NaCl (Gerdemann et al., 2007). Other experiments showed precipitation of magnesite on the surface of forsterite crystals in a solution of $MgCl_2$ + $NaHCO_3$ at 95 °C and P_{CO2} = 100 bar (Giammar et al., 2005). The forsterite had been reacted for 10 days, but indications of magnesite precipitation were detected after less than 3 days. Even fewer labs have succeeded in demonstrating olivine carbonation without manipulating the reaction conditions. Batch reactor experiments have been performed on crushed olivine in aqueous solutions equilibrated with supercritical CO_2 at 150 °C and total pressure of 150 bar. A magnesite yield, as high as 57 ± 2%, was obtained after a 1 month of incubation time (Garcia et al., 2010).

One limitation for observing mineral reactivity with classical macroscopic techniques is that it takes a very long time for slow reactions to produce enough secondary phases to be visible, such as with the traditional tools of geochemistry: X-ray diffraction (XRD) and electron microprobe (EM). Techniques designed for observation at the nanometer scale offer the possibility of seeing changes after minutes to hours, that would take days, years or centuries to observe using classical methods. AFM provides detailed information about the physical character of surfaces, such as topography, roughness, adhesion properties and elasticity, but only a few AFM studies have been performed on olivine. Among those, AFM has been applied to monitor the real time dissolution rate of olivine in nitric acid (Heaton and Engstrom, 1994). In more recent work, olivine was ion irradiated to simulate the effects of interstellar gas-grain interactions and its morphological evolution was investigated with AFM (Davoisne et al., 2008).

The purpose of this study was to apply surface sensitive techniques, such as AFM, SEM and XPS, to examine olivine crystals and its reaction products. We compared the composition and character of freshly fractured crystals with samples exposed to CO_2 under various pressure and temperature conditions to determine what secondary products are likely to form, where they form and what differences there are when conditions are changed.

2. EXPERIMENTAL DETAILS

2.1 Preparation of Olivine Samples for Analysis

All experiments were performed on olivine crystals picked from a peridotite nodule acquired from the Geological Museum of Copenhagen. The origin of the nodule is unknown and therefore it was extensively characterized with classical analytical methods, including powder X-ray diffraction, electron microprobe and polarized light microscopy on polished thin sections. The nodule was not serpentinized and was somewhat friable, so light crushing dissociated the individual mineral grains. Crystals were examined with a reflected light microscope and separated with tweezers to provide monomineral samples for further analysis (Fig. 1a). Those with visible inclusions of other minerals were not included.

For examination with nanoscale techniques, we used atomic force microscopy (AFM), X-ray photoelectron spectroscopy (XPS) and scanning electron microscopy (SEM). Clean tools and working conditions are crucial when only the top few atomic layers are accessible for analysis. Fresh olivine surfaces were obtained by applying force to selected, individual olivine crystals until they fractured into smaller pieces. When subjected to mechanical stress, olivine displays conchoidal fracture; i.e. it does not break along prominent cleavage directions. Samples were fractured immediately before the beginning of experiments to be sure which surface was the fresh one and to minimize the accumulation of air-borne contamination called adventitious carbon (Stipp and Hochella, 1991). Mineral fragment dust was removed from the fresh surfaces with a jet of 99.999% pure nitrogen and when possible, surfaces were examined with AFM before further

experiments were performed. Powders were obtained by crushing handpicked olivine crystals in a clean agate mortar until the particles were approximately 50 μm in diameter.

All olivine samples were reacted for 4 days unless otherwise stated. Samples reacted with air (results presented in Section 3.2) were stored in a clean plastic Petri dish with the cover on. The lack of a seal allowed air to exchange outside the dish but dust contamination was minimised. Freshly fractured olivine crystals treated with water (results in Section 3.3) were stored individually, in closed 25 ml Teflon beakers completely filled with MilliQ water, i.e., no head space.

All high P-T reaction experiments where oxygen was present (results in Section 3.4.1 and Section 3.4.2) were carried out in a 500 ml capacity 4650, high quality stainless steel, high pressure vessel with a 4836 temperature controller from Parr Instruments. The reaction vessel was loaded with 100 ml MilliQ water and an open 25 ml Teflon beaker to hold the sample. The sample was either ~0.3 grams of fresh crushed olivine powder or 30-35 individual, fresh olivine crystal fragments weighing ~0.05 grams in total. For experiments where the olivine was reacted at increased CO_2 partial pressure, the reaction vessel was charged with CO_2 until 50 bars was reached, before sealing. The reaction vessel was kept at room temperature or heated to 120 °C, which increased the total pressure. The concentration of oxygen inside the reactor during these experiments was estimated to be ~3.4 parts per thousand.

All sample preparations for the oxygen deficient experiments (results presented in Section 3.4.3) were conducted inside a glove box supplied by Coy Laboratory Products. This soft walled PVC chamber was slightly overpressured with pure carbon dioxide containing a few percent of hydrogen in order to remove oxygen catalytically as water on palladium pellet filters. At all times during these experiments, the oxygen level was measured to be <20 ppm by the Coy Combined Oxygen and Hydrogen Analyzer. Oxygen deficient, high P-T reaction experiments were carried out in a 600 ml 4568 High Pressure Vessel with a 4843 Temperature Controller from Parr Instruments. The sample and 100 ml of MilliQ water that had been boiled to exsolve dissolved oxygen, were transferred from the glove box into the reactor without exposure to air. The reactor containing the sample was evacuated for 5 minutes and subsequently purged with 100% CO_2 for 5 minutes more. The CO_2 pressure was then increased to 50 bars and the reactor was closed and heated to 120 °C, which increased the total pressure.

The crystals that had been reacted in the presence and absence of oxygen were rinsed individually with MilliQ water for 2-3 seconds and dried with a jet of N_2. The red precipitate that covered the olivine fragments after reaction was removed from some of the reacted crystals and suspended by placing them into ethanol for 1 hour. The suspension was transferred to a glass slide and dried under a lamp. The precipitate was identified by XRD. Reacted powders were extracted from the liquid by centrifuging for 5 minutes at 5000 rpm, decanted and dried for 24 hours in a Christ Alpha 1-2 LD freeze dryer. An overview of the reaction conditions for all experiments is presented in Table 1.

2.2 Characterization Techniques and Parameters

For identifying the crystal phases, we used X-ray diffraction. Patterns were collected in a Bruker D8 Advance X-ray Diffractometer in Bragg-Brentano geometry, equipped with a Cu-Kα radiation source and a germanium monochromator. Scans were taken for 2θ ranging from 2° to 70° with 2°/s steps. For identifying the red reaction products formed on the olivine surfaces, the 2θ ranges and step sizes were changed to 4° to 92° and 0.02°/s. All XRD samples were compared with the powder diffraction standards in the PDF-2 file for mineral identification (International Center for Diffraction Data, 1995).

For examining rock thin sections with polarized light microscopy, we used a Zeiss AXIO Imager A1m Laboratory Microscope. For electron microprobe, polished sections were coated with about 10 nm of carbon using a JEOL (JEC 560) Auto Carbon Coater. The quantitative chemical microprobe analysis was conducted with a JEOL-microprobe (JXA-8200) operating with an accelerating voltage of 15 kV and a beam current of 15 nA. The elements were analyzed using their Kα spectrum lines and for standards we used natural and synthetic silicates and oxides. The counting time was 10 s, except for Ni, present in trace quantities, where it was 40 s. For defining the Mg and Fe ion concentrations in the olivine, we used a Perkin-Elmer 5100 atomic absorption spectroscope (AAS), running in flame mode. The olivine crystals were first dissolved in a mixture of hydrofluoric acid (HF) and nitric acid (HNO_3). The solution was evaporated and the dry precipitate was redissolved in 10 ml 7 M hydrochloric acid (HCl).

The surface morphology of the samples was investigated with an atomic force microscope (AFM). We used a Digital Instruments Multimode IIIa operated in contact mode with standard silicon nitride tips. Crystal samples were fixed on a circular steel stub with modelling clay (plasticine) so the freshly prepared, concoidal fracture surface could be set as horizontally as possible. AFM provides images with lateral resolution ranging from several micrometers to fractions of a nanometer and vertical resolution ranging from about a half micrometer to fractions of a nanometer. X-ray photoelectron spectroscopy (XPS) was used to investigate the chemical composition, element distribution, and electronic state of the top atomic layers of the olivine. Lateral spot size is about 500 µm but vertical information depth is about 10 nm. All XPS analyses were conducted with a Kratos AXIS Ultra instrument using a monochromatised $Al_{K\alpha}$ X-ray anode and slow electron charge compensation. The survey spectra were made with pass energy of 160 eV, with a 0.5 eV step size and step time of 22 ms. The XPS data were processed by the CasaXPS software using the Shirley background removal (Shirley, 1972).

For transmission electron microscopy (TEM), the reacted powders were dispersed in MilliQ, ground in an agate mortar and floated onto a polymer coated Cu grid. The powder was analyzed using a Phillips CM20 instrument, operating at 200 kV. Scanning electron microscopy (SEM) images were collected with FEI Inspect S50 running in secondary electron mode at 5.0 kV. SEM samples were coated using a 208HR Sputter Coater from Cressington, with about 12 nm of Pt/Pd.

3. RESULTS AND DISCUSSION

3.1. The Olivine Sample

The peridotite nodule contained four main minerals, which we differentiated by colour, luster and crystal form (Fig. 1a), and confirmed with X-ray powder diffraction to be: a light green olivine (~83% by weight), a brown green enstatite (~10%), a dark green aluminium rich diopside (~7%) and a black brown spinel (<1%) (Fig. 1a). Their elemental composition was established quantitatively with microprobe analysis (Table 2). Also present were minor amounts (<1%) of iron and nickel sulfide phases: pentlandite, pyrrhotite and pyrite, as expected in a peridotite. Chromium was present in the spinel. The olivine crystals contained small amounts of nickel, calcium, manganese, aluminium and traces of titanium in addition to the typical major elements (Table 2). These are all common constituents of olivine from ultramafic rocks (Smith, 1966; Deer et al., 1997). Based on the atomic absorption spectroscopy measurements and the microprobe analyses, the olivine was identified as low Fe forsterite ($Fo_{91.1}$).

A thin section analysis showed that the primary minerals were almost unaltered (Fig. 2). The olivine was present in large grains while the pyroxenes were smaller and fractured. The nodule contained no feldspar. In the primary minerals, there was evidence of two generations of old liquid or gas penetration, possibly CO_2 or H_2O from the melt, in the form of aligned bubbles. These indicated that the gas inclusions had been caught and isolated along old crystal cracks in the healing process, during or after a deformation stage. The bubbles had a pseudo crystal form, i.e., negative crystals, and some of the cavities were empty while others contained fluid. Inclusions of carbonaceous liquid and

gas have previously been reported in olivine nodules from all over the world (Roedder, 1965; Mathez, 1987; Tingle et al., 1991). In the experiments described in the following sections, olivine was the only crystal phase reacted.

3.2. Olivine Reaction in Air

AFM showed that features formed during reaction of the freshly fractured olivine surfaces were often aligned parallel (Table 1, Ex01). Some features had concave or convex form, arranged in a regular pattern, such as the bumps seen in Figure 3a. This feature is somewhat atypical of the surfaces we observed; we have interpreted it as a regular series of linear dislocations that probably developed on a subgrain boundary. Such dislocations are not uncommon in olivine (Blacic and Christie, 1973). Some of the freshly fractured olivine surfaces reacted spontaneously in air within 4 hours of exposure. The reaction products formed as a homogeneous layer of bumps that were approximately equal in shape and size (Fig. 3b) and that also displayed a weak parallel lineation. The reaction products had a half spherical form with diameter <100 nm, but their size increased with time. They grew continuously but their growth rate decreased with time during the 30 days that the crystal surfaces were observed. In contrast, some olivine faces displayed only a very limited alteration during more than 30 days of exposure to air. This suggests that the orientation of the fracture relative to the crystallographic axes of the olivine exposes different atomic arrangements that vary in their reactivity.

Some surfaces, immediately after fracture, such as Figure 3c, are already covered by abundant small features. Their form and size are heterogeneous. They are similar in

appearance to the features formed by the secondary products observed during reaction with air. Because they are present as soon as the crystals are fractured, we interpreted these original, heterogeneous features to be reaction products that had formed on old fractures as the minerals reacted with migrating fluids. Old cracks are weaker than the surrounding crystal, so it is not a surprise that they open, exposing old secondary minerals. Such reacted fractures have been reported before (Roedder, 1965; Mathez, 1987; Tingle et al., 1990; Tingle et al., 1991). XPS measurements from fractured crystals, and from olivine powder produced by grinding so that the new surfaces produced were fresh rather than opened old fractures, supported this hypothesis (Table 1, Ex02). All spectra confirmed the elements expected for olivine: magnesium, iron, silicon and oxygen (Table 3, Ex02), but peaks were present for two elements that are alien to olivine, namely, aluminium and carbon. Aluminium can easily be explained by tiny spinel and pyroxene inclusions. The presence of a much higher proportion of carbon on the olivine fractures than on the freshly ground powder is evidence that a large fraction of the carbon originated in the peridotite sample itself, such as on the fractures in the olivine observed in Figure 2. This interpretation is consistent with previous reports of carbon observed with XPS on olivine surfaces. This carbon signal could be diminished by polishing or cleaning (Mathez, 1987; Seyama et al., 1996; Davoisne et al., 2008). A smaller amount of carbon is also found on new, fresh fractures both immediately after they are formed and after the samples has been exposed to liquid, such as we see on the crushed powder (Table 3). This is adventitious carbon, contamination that comes from air. It is not possible to remove the contamination signal completely; it returns instantly as soon as the sample is exposed to air.

3.3. Olivine Reaction in Water

AFM imaging of olivine crystals exposed to pure water (MilliQ) at equilibrium with the CO_2 in air revealed significant surface changes (Table 1, Ex03). Dissolution was obvious and new products formed within hours to days. The features produced (Fig. 4a) became larger and more distinct with time. Some surfaces exposed to water became covered with loosely bound material that could be easily scraped away with the AFM tip without applying additional force. Scanning the same area several times scraped the surface material to the sides of the scanning frame (Fig. 4b) and uncovered the surface below. The underlying surface appeared similar to other dissolved olivine surfaces and did not change further with continued scraping, even after two hours, or with increased force on the AFM tip. The loose material could be partly dissolved olivine, i.e. the silica residue remaining as Mg and Fe are leached to solution, or it could be silica or other secondary phases that have reprecipitated from the solution in contact. Surface features and the extent of alteration were different on different surfaces, as we saw with reaction in air, suggesting that crystallographic orientation controls reactivity. Dissimilarities in the dissolution rates of olivine faces have been reported previously (Grandstaff, 1978; Awad et al., 2000).

AFM and SEM investigations revealed several interesting features on the olivine surfaces exposed to MilliQ water. New rod shaped units with uniform dimensions appeared at random orientations, in clusters, after about 4 days of water exposure, and after 10 days few areas remained unpopulated (Fig. 4c). The rods were consistently about 3 μm long,

700 nm wide and 110 nm high. Their regularity of size and length to width ratio is abnormal for mineral crystallites and they resembled features in other images of surfaces that had been inoculated with bacteria. Surfaces of crystals boiled in water for 4 days remained free of them. It is likely that these bacteria were lithotrophic organisms exploiting the energy gained from oxidizing Fe^{2+} to assimilate carbon (Cornell and Schwertmann, 2003).

Increasing the temperature for samples exposed to water led to increased rates of dissolution and recrystallization (Table 1, Ex04). Crystals that reacted with water for 4 days at 120 °C in a Teflon beaker turned red, indicating iron oxide coatings. When Fe^{2+} is released from the olivine substrate, it is gets oxidized by the air trapped in the reaction vessel and iron oxide phases precipitate. Unfortunately, it was not possible to get an XRD pattern from this red coating; although it was clearly visible, there was too little material for analysis.

3.4. Olivine in Water at Increased CO_2 Pressures

3.4.1 Reaction at Room Temperature

Extensive surface alteration was observed on olivine fragments reacted with water and CO_2 at room temperature and CO_2 partial pressures increased to 50 bars (Table 1, Ex05). AFM images demonstrated that surface appearance varied over the surface, i.e. it was locally variable at a scale of micrometers. A common feature was identically oriented fibres or pinnacles protruding at an angle from the olivine surface (Fig. 5).

The observed features could either be secondary minerals growing from the surface, or they could arise from the original sample as portions that dissolve more slowly than the surrounding olivine. Dislocations are known to have different dissolution properties than the parent crystal so the first possibility is that the observed surfaces features are the ends of subparallel linear dislocations. This would explain the angle to the surface and alignment of the fibres. Alternatively, the features might be fibres that grow out of the surface. Olivine is a solid solution of Mg and Fe end members, but distribution of cations might not be completely random, causing slight differences in local solubility. Local composition variation might be correlated with the set of parallel dislocations present in the mineral (Putnis, 1992) as a result of exchange processes taking place along these dislocations. Dissolution would produce a surface with high spots. These could act as nucleation sites for the growth of secondary minerals, which would further inhibit dissolution. Orientation at an angle to the surface can easily be explained by the orientation of locally enriched or depleted olivine.

Anisotropic dissolution and formation of isolated pinnacles on acid treated olivine surfaces have previously been observed with SEM by Grandstaff (Grandstaff, 1978). In his experiments, the pinnacles were about 10 times larger than the features we describe here. In contrast with our study, he proposed that material bordering dislocations would preferentially be removed so the pinnacles represent material isolated between intersecting dislocation planes. From the data we have collected, as well as Grandstaff's results, we propose that the most consistent interpretation is slightly less soluble zones in the olivine crystal.

3.4.2 Reaction at 120 °C

The surface of some of the olivine crystal faces was faintly red after less than 15 hours of reaction in pure water equilibrated with supercritical CO_2 at total pressure 70-80 bars. Increasing the reaction time to 4 days yielded crystals covered with a red precipitate (Fig. 1b) (Table 1, Ex06). TEM images of reacted olivine powder showed many large fragments covered by layers that have parallel aligned, fibrous texture (Fig. 6). We interpret these as unaltered olivine cores with loose surface reaction products. An XRD analysis of the reacted powder provided only an olivine pattern with no evidence of an iron oxide phase. This is easy to explain. The red coating is a very small fraction of the mineral volume and is probably not well crystallized. XPS data from a reacted sample, Ex06 Powder, compared with data from the unreacted control, Ex02 Powder, show a dramatic change in surface composition after reaction (Table 3). There was more iron and oxygen, but less magnesium. AAS measurements of the reacted solution revealed 10 mg/l Mg concentration whereas Fe was below the detection limit (μg/l). Such low Fe concentrations are expected when soluble Fe(II) is oxidized to insoluble Fe(III) and forms iron (hydr)oxides.

XPS measurements of single crystals reacted in the same vessel as crushed olivine powder, Ex06 Crystals 2, showed only an increase in Si and O suggesting either leaching of cations, which formed secondary phases elsewhere, or the formation of silica/silicates that covered the crystal surfaces (Table 3). SEM images from reacted crystals revealed several types of reaction products (Fig. 7). Some regions showed a newly formed, flat compound that homogenously covered large areas of the crystal surface (Fig. 7a). It

exfoliated in large flakes to reveal rounded particles underneath, some almost perfectly spherical (Fig. 7a, b and c). The flakes are likely to be secondary phyllosilicates and the morphology of the spherical particles is reminiscent of amorphous silica formed under similar reaction conditions, reported previously (Potapov, 2004; Béarat et al., 2006; Gaillou et al., 2008). A third compound is present as long rods (Fig. 7b, d, and e). These are aligned in a grid and are oriented consistently, probably controlled by the orientation of the olivine. These observations reinforce the anisotropic behaviour of the various olivine faces. It has previously been reported that the growth of smectite and hematite (Banfield et al., 1991) and smectite and goethite (Eggleton, 1984; Smith et al., 1987) are influenced by the structure and orientation of the parent olivine crystal. The best explanation is that the long rods are a network of dissolution resistant dislocations (e.g., decorated by magnetite), which remain when the surrounding olivine is leached away.

XRD analysis of the reaction products showed peaks for magnesite and principal peaks of hematite and magnesian calcite (Fig. 8). A parallel run produced hydromagnesite as well. The broad scattering intensity around 22° 2θ is characteristic for amorphous silica as a reaction product but a blank run revealed that it represents the glass sample substrate. This is one of first studies in which magnesite has been observed to form directly on olivine crystals, without the presence of additional salts to supersaturate the reaction solution. Giammar and collegues (Giammar et al., 2005) also observed a red brown phase forming on CO_2-reacted olivine crystals under similar conditions, but could not identify it. Garcia et al. (Garcia et al., 2010) reported magnesite formation on olivine grains but at

more extreme conditions, i.e. 150 °C and total pressure of 150 bar and longer reactions times of 2-8 weeks.

3.4.3 Oxygen Deficient Reaction at 120 °C

To optimize carbon capture, the number of cations available for reaction ought to be maximized, so formation of Fe oxides should be minimized by keeping iron reduced as Fe(II). Presence of Fe(II) and CO_3^{2-} and slightly basic pH is expected to promote the formation of siderite, $FeCO_3$, fixing the carbon as a relatively insoluble mineral and at the same time, decreasing the concentration of dissolved Fe(II), promoting further dissolution of olivine. There was very little oxygen in our experiments and we made a second set of experiments to ensure oxygen deficient conditions. The experimental setup limited the run pressure to about 15 bars lower than during the previous experiments where conditions were subcritical with respect to CO_2 (Table 1, Ex07). After reaction, the crystals produced in the oxygen deficient experiments were covered with a red product that was slightly brighter than the colour obtained in the experiments with oxygen present, suggesting a difference either in the particle size or identity of the secondary phase. An XRD pattern of the product gave a best match for forsterite, magnesian calcite and hematite (Fig. 8). The absence of magnesite in the oxygen deficient experiments is attributed to lower reaction pressures compared with the experiments conducted with supercritical CO_2 conditions, described in the previous section.

XPS confirmed the presence of iron oxides on reacted crystal and powder samples (Table 3). The XPS O (1s) peaks for the supercritical CO_2 (Ex06 Powder) and the oxygen deficient (Ex07 Powder) reacted powders were different from the fresh olivine control

(Ex02 Powder) (Fig. 9). The original material gave a wide and slightly asymmetrical peak, reflecting the presence of more than one type of O bond. Broadening of the O (1s) peak after reaction represents change in the relative abundance of these bonding environments and shows that new secondary phases with a different O (1s) environment have developed. Peak extension toward higher binding energy, such as Ex06 Powder, indicates the presence of silica, clay or carbonate minerals, while a broadening toward a lower binding energy, such as Ex07 Powder, indicates the presence of iron oxides (Moulder et al., 1995). The O (1s) peaks for both the reacted olivine experiments are shifted toward a higher binding energy, suggesting an increase in the relative proportion of silicates or carbonates.

SEM images of the olivine reacted in the system where oxygen was absent revealed heavily deteriorated surfaces with extensive dissolution features (Fig. 10a). Etch pits and gaping troughs were common, probably induced by lattice imperfections such as dislocations, cleavage planes or fractures (Grandstaff, 1978; Béarat et al., 2006). The surfaces had slightly less and different looking reaction products than what we observed for the supercritical CO_2 experiments presented in the previous section. Scattered and isolated needle-like crystals were observed on bare olivine regions. They were generally 1-2 μm long and about 100 nm thick, which is characteristic for goethite (Cornell and Schwertmann, 2003). This agrees with the presence of star twins of up to three individuals (Fig. 10b, insert). The needles were commonly observed in clusters, associated with rosettes that had a diameter of about 800 nm (Fig. 10c). The rosettes are intergrowths of several flaky individual crystals. These networks of secondary products

sometimes bordered topographic steps on the olivine substrate, indicating that dissolution of the host crystal occurred along preferential directions and its dissolution fed the development of the secondary products directly (Fig. 10b). The formation of iron oxides in the oxygen free environment might be evidence for water cleavage into oxygen and hydrogen, with oxygen being consumed, as presumed for serpentinization, which creates magnetite and secondary Mg silicates (McCollom and Bach, 2009). Instant precipitation of iron oxide upon exposure to air is not likely because this would have generated a homogenous layer and neither goethite nor hematite can crystallize in a few minutes. It is not likely that the iron oxides result from corrosion of the high pressure vessel walls. The olivine samples and solutions were isolated inside covered Teflon beakers; the reaction vessels were built of the most resistant stainless steel that can be purchased; and there was no sign of corrosion on the vessel walls.

Previous researchers have suggested that an Fe layer that formed on olivine surfaces could inhibit olivine dissolution (Schott and Berner, 1983; Wogelius and Walther, 1992). Others conclude that discrete precipitated particles do not limit dissolution (Giammar et al., 2005; Stockmann et al., 2011). Our results clearly indicate a layer of secondary phases which could decelerate the olivine carbonation process, but over the duration of our experiments, there is not enough evidence to say that it would stop it completely.

4. CONCLUSIONS AND IMPLICATIONS

Olivine crystals contain cracks with coatings of carbon and abundant evidence of reaction in the form of secondary phases. Fresh olivine fractures are smooth and conchoidal but they react almost instantly, forming new reaction products during exposure to air. Fresh olivine exposed to water dissolves and secondary phases form. Samples that remain in water for more than 4 days, rod shaped bacteria appear that might have been lithotrophs, living from the Fe redox transition. A loosely attached, reacted layer forms on the olivine surface in contact with water, that can be scraped away with the AFM tip. Formation of a soft layer is consistent with the leaching of Mg and Fe, leaving silica behind. The rate of surface alteration depends on the orientation of the olivine crystal surface.

At elevated temperatures and increased CO_2 pressure, olivine suffers extensive deterioration and red or red brown secondary phases form on its surfaces. These were identified by XRD and XPS as hematite and carbonate minerals. Even in the absence of oxygen, iron is oxidized, so iron oxides must form by the conversion of H_2O to ½ O_2 and H_2 (Evans, 2010; Müntener, 2010). What is remarkable in our experiments is that we consistently produce hematite and not the usual magnetite, probably because of the increased temperature. McCollom and Bach (McCollom and Bach, 2009) suggest that at 150 °C, iron escapes into brucite and that the optimal conditions for producing H_2 and Fe oxides is in the temperature range of 200-315 °C. We have observed that such reactions are also possible at 120 °C. The formation of iron oxides competes with the process of carbonation, consuming some of cations released from the olivine that could be used to sequester CO_3^{2-} and producing H_2 which is undesirable. The experimental and practical

challenge is how to inhibit hydrolysis, so as to maintain high concentrations of Fe(II) and optimize precipitation of $FeCO_3$, instead.

The investigation of olivine with surface sensitive techniques provides new insight into the processes important for carbonation. With these techniques, nanoscale details about the processes of dissolution, the formation of secondary products and their identity, and the effect of these reactions on carbonation. The results obtained at pressures and temperatures relevant for CO_2 sequestration are useful for setting up models to predict the processes that are likely to take place, e.g. when CO_2 is injected into porous basalt and ultramafic rocks, and to assess the potential for carbon sequestration.

Acknowledgments We are grateful to Keld West, Caroline Piper Hem, Flemming Hansen, Helene Almind, Alfons Berger, Karina Krarup Sand, Knud Dideriksen, Sorin Nedel, Vagn Moser and members of the NanoGeoScience group at the University of Copenhagen for comments and discussion. The NanoGeoScience laboratory was established by a grant from the Danish National Natural Sciences Research Council (FNU).

References

Alfredsson H. A., Hardarson B. S., Franzson H. and Gislason S. R. (2008) CO_2 sequestration in basaltic rock at the Hellisheidi site in SW Iceland: stratigraphy and chemical composition of the rocks at the injection site. *Mineral. Mag.* **72**, 1-5.

Andreani M., Luquot L., Gouze P., Godard M., Hoisé E. and Gibert B. (2009) Experimental study of carbon sequestration reactions controlled by the percolation of CO_2-rich brine through peridotites. *Environ. Sci. Technol.* **43**, 1226-1231.

Awad A., van Groos A. F. K. and Guggenheim S. (2000) Forsteritic olivine: effect of crystallographic direction on dissolution kinetics. *Geochim. Cosmochim. Acta* **64**, 1765-1772.

Banfield J. F., Jones B. F. and Veblen D. R. (1991) An AEM-TEM study of weathering and diagenesis, Abert Lake, Oregon: I. weathering reactions in the volcanics. *Geochim. Cosmochim. Acta* **55**, 2781-2793.

Béarat H., McKelvy M. J., Chizmeshya A. V. G., Gormley D., Nunez R., Carpenter R. W., Squires K. and Wolf G. H. (2006) Carbon sequestration via aqueous olivine mineral carbonation: role of passivating layer formation. *Environ. Sci. Technol.* **40**, 4802-4808.

Blacic J. D. and Christie J. M. (1973) Dislocation substructure of experimentally deformed olivine. *Contrib. Mineral. Petrol.* **42**, 141-146.

Brady P. V. and Gíslason S. R. (1997) Seafloor weathering controls on atmospheric CO_2 and global climate. *Geochim. Cosmochim. Acta* **61**, 965-973.

Chen Z.-Y., O'Connor W. K. and Gerdemann S. J. (2006) Chemistry of aqueous mineral carbonation for carbon sequestration and explanation of experimental results. *Environ. Prog.* **25**, 161-166.

Cornell R. M. and Schwertmann U. (2003) *The iron oxides: structure, properties, reactions, occurrences and uses*. Wiley-VCH, Weinheim.

Daval D., Sissmann O., Menguy N., Saldi G. D., Guyot F., Martinez I., Corvisier J., Garcia B., Machouk I., Knauss K. G. and Hellmann R. (2011) Influence of amorphous silica layer formation on the dissolution rate of olivine at 90 °C and elevated pCO_2. *Chem. Geol.* **284**, 193-209.

Davoisne C., Leroux H., Frère M., Gimblot J., Gengembre L., Djouadi Z., Ferreiro V., d'Hendecourt L. and Jones A. (2008) Chemical and morphological evolution of a silicate surface under low-energy ion irradiation. *Astron. Astrophys.* **482**, 541-548.

Deer W. A., Howie R. A. and Zussman J. (1997) *Orthosilicates*. Geological Society of London, London.

Eggleton R. A. (1984) Formation of iddingsite rims on olivine: a transmission electron microscope study. *Clays Clay Miner.* **32**, 1-11.

Evans B. W. (2010) Lizardite versus antigorite serpentinite: magnetite, hydrogen, and life(?). *Geology* **38**, 879-882.

Gaillardet J., Dupre B., Louvat P. and Allegre C. J. (1999) Global silicate weathering and CO_2 consumption rates deduced from the chemistry of large rivers. *Chem. Geol.* **159**, 3-30.

Gaillou E., Fritsch E., Aguilar-Reyes B., Rondeau B., Post J., Barreau A. and Ostroumov M. (2008) Common gem opal: an investigation of micro- to nano-structure. *Am. Mineral.* **93**, 1865-1873.

Garcia B., Beaumont V., Perfetti E., Rouchon V., Blanchet D., Oger P., Dromart G., Huc A. Y. and Haeseler F. (2010) Experiments and geochemical modelling of CO_2 sequestration by olivine: potential, quantification. *Appl. Geochem.* **25**, 1383-1396.

Gerdemann S. J., O'Connor W. K., Dahlin D. C., Penner L. R. and Rush H. (2007) Ex situ aqueous mineral carbonation. *Environ. Sci. Technol.* **41**, 2587-2593.

Giammar D. E., Bruant R. G. and Peters C. A. (2005) Forsterite dissolution and magnesite precipitation at conditions relevant for deep saline aquifer storage and sequestration of carbon dioxide. *Chem. Geol.* **217**, 257-276.

Gislason S. R., Wolff-Boenisch D., Stefansson A., Oelkers E. H., Gunnlaugsson E., Sigurdardottir H., Sigfusson B., Broecker W. S., Matter J. M., Stute M., Axelsson G. and Fridriksson T. (2010) Mineral sequestration of carbon dioxide in basalt: a pre-injection overview of the CarbFix project. *Int. J. Greenh. Gas Control* **4**, 537-545.

Goldberg D. S., Takahashi T. and Slagle A. L. (2008) Carbon dioxide sequestration in deep-sea basalt. *Proc. Natl. Acad. Sci. U. S. A.* **105**, 9920-9925.

Goldberg P., Chen Z.-Y., O'Connor W., Walters R. and Ziock H.-J. (2001) CO_2 mineral sequestration studies in US. In: *Proceedings of the First National Conference on Carbon Sequestration*. National Energy Technology Laboratory, Washington, DC.

Grandstaff D. E. (1978) Changes in surface area and morphology and the mechanism of forsterite dissolution. *Geochim. Cosmochim. Acta* **42**, 1899-1901.

Hänchen M., Prigiobbe V., Baciocchi R. and Mazzotti M. (2008) Precipitation in the Mg-carbonate system - effects of temperature and CO_2 pressure. *Chem. Eng. Sci.* **63**, 1012-1028.

Hänchen M., Prigiobbe V., Storti G., Seward T. M. and Mazzotti M. (2006) Dissolution kinetics of fosteritic olivine at 90-150 °C including effects of the presence of CO_2. *Geochim. Cosmochim. Acta* **70**, 4403-4416.

Heaton J. S. and Engstrom R. C. (1994) In situ atomic force microscopy study of the differential dissolution of fayalite and magnetite. *Environ. Sci. Technol.* **28**, 1747-1754.

International Center for Diffraction Data (1995) *PDF-2 Sets 1-45 database*, Newtown Square, PA 19073, USA.

Jarvis K., Carpenter R. W., Windman T., Kim Y., Nunez R. and Alawneh F. (2009) Reaction mechanisms for enhancing mineral sequestration of CO_2. *Environ. Sci. Technol.* **43**, 6314-6319.

Kelemen P. B. and Matter J. (2008) In situ carbonation of peridotite for CO_2 storage. *Proc. Natl. Acad. Sci. U. S. A.* **105**, 17295-17300.

King H. E., Plümper O. and Putnis A. (2010) Effect of secondary phase formation on the carbonation of olivine. *Environ. Sci. Technol.* **44**, 6503-6509.

Kump L. R., Brantley S. L. and Arthur M. A. (2000) Chemical, weathering, atmospheric CO_2, and climate. *Annu. Rev. Earth Planet. Sci.* **28**, 611-667.

Lackner K. S., Wendt C. H., Butt D. P., Joyce E. L. and Sharp D. H. (1995) Carbon dioxide disposal in carbonate minerals. *Energy* **20**, 1153-1170.

Mathez E. A. (1987) Carbonaceous matter in mantle xenoliths: composition and relevance to the isotopes. *Geochim. Cosmochim. Acta* **51**, 2339-2347.

Matter J. M. and Kelemen P. B. (2009) Permanent storage of carbon dioxide in geological reservoirs by mineral carbonation. *Nat. Geosci.* **2**, 837-841.

Matter J. M., Takahashi T. and Goldberg D. (2007) Experimental evaluation of in situ CO_2-water-rock reactions during CO_2 injection in basaltic rocks: implications for geological CO_2 sequestration. *Geochem. Geophys. Geosyst.* **8**.

McCollom T. M. and Bach W. G. (2009) Thermodynamic constraints on hydrogen generation during serpentinization of ultramafic rocks. *Geochim. Cosmochim. Acta* **73**, 856-875.

McGrail B. P., Schaef H. T., Ho A. M., Chien Y. J., Dooley J. J. and Davidson C. L. (2006) Potential for carbon dioxide sequestration in flood basalts. *J. Geophys. Res.-Solid Earth* **111**.

Morrow C. P., Kubicki J. D., Mueller K. T. and Cole D. R. (2010) Description of Mg^{2+} release from forsterite using ab initio methods. *J. Phys. Chem. C* **114**, 5417-5428.

Moulder J. F., Stickle W. F., Sobol P. E. and Bomben K. D. (1995) *Handbook of X-ray Photoelectron Spectroscopy*. Physical Electronics, Minnesota.

Müntener O. (2010) Serpentine and serpentinization: a link between planet formation and life. *Geology* **38**, 959-960.

Oelkers E. H. (2001) An experimental study of forsterite dissolution rates as a function of temperature and aqueous Mg and Si concentrations. *Chem. Geol.* **175**, 485-494.

Oelkers E. H., Gislason S. R. and Matter J. (2008) Mineral Carbonation of CO_2. *Elements* **4**, 333-337.

Pokrovsky O. S. and Schott J. (2000a) Forsterite surface composition in aqueous solutions: a combined potentiometric, electrokinetic, and spectroscopic approach. *Geochim. Cosmochim. Acta* **64**, 3299-3312.

Pokrovsky O. S. and Schott J. (2000b) Kinetics and mechanism of forsterite dissolution at 25 °C and pH from 1 to 12. *Geochim. Cosmochim. Acta* **64**, 3313-3325.

Potapov V. V. (2004) Formation of solid deposits of amorphous silica in a flow of hydrothermal solution. *Glass Phys. Chem.* **30**, 82-89.

Prasad P. S. R., Sarma D. S., Sudhakar L., Basavaraju U., Singh R. S., Begum Z., Archana K. B., Chavan C. D. and Charan S. N. (2009) Geological sequestration of carbon dioxide in Deccan basalts: preliminary laboratory study. *Curr. Sci.* **96**, 288-291.

Putnis A. (1992) *Introduction to mineral sciences*. Cambridge University Press, Cambridge.

Roedder E. (1965) Liquid CO_2 inclusions in olivine-bearing nodules and phenocrysts from basalts. *Am. Mineral.* **50**, 1746-1782.

Rosso J. J. and Rimstidt J. D. (2000) A high resolution study of forsterite dissolution rates. *Geochim. Cosmochim. Acta* **64**, 797-811.

Schaef H. T., McGrail B. P. and Owen A. T. (2009) Basalt-CO_2-H_2O interactions and variability in carbonate mineralization rates. *Energy Procedia* **1**, 4899-4906.

Schopka H. H., Derry L. A. and Arcilla C. A. (2011) Chemical weathering, river geochemistry and atmospheric carbon fluxes from volcanic and ultramafic regions on Luzon Island, the Philippines. *Geochim. Cosmochim. Acta* **75**, 978-1002.

Schott J. and Berner R. A. (1983) X-ray photoelectron studies of the mechanism of iron silicate dissolution during weathering. *Geochim. Cosmochim. Acta* **47**, 2233-2240.

Schott J., Pokrovsky O. S. and Oelkers E. H. (2009) The link between mineral dissolution/precipitation kinetics and solution chemistry. In: *Thermodynamics and Kinetics of Water-Rock Interaction*. Mineralogical Society of America, Chantilly.

Seyama H., Soma M. and Tanaka A. (1996) Surface characterization of acid-leached olivines by X-ray photoelectron spectroscopy. *Chem. Geol.* **129**, 209-216.

Shirley D. A. (1972) High-resolution X-ray photoemission spectrum of valence bands of gold. *Phys. Rev. B* **5**, 4709-4714.

Smith J. V. (1966) X-ray-emission microanalysis of rock-forming minerals. II. Olivines. *J. Geol.* **74**, 1-16.

Smith K. L., Milnes A. R. and Eggleton R. A. (1987) Weathering of basalt: formation of iddingsite. *Clays Clay Miner.* **35**, 418-428.

Stipp S. L. and Hochella M. F. (1991) Structure and bonding environments at the calcite surface as observed with X-ray photoelectron spectroscopy (XPS) and low energy electron diffraction (LEED). *Geochim. Cosmochim. Acta* **55**, 1723-1736.

Stockmann G. J., Wolff-Boenisch D., Gislason S. R. and Oelkers E. H. (2011) Do carbonate precipitates affect dissolution kinetics? 1: basaltic glass. *Chem. Geol.* **284**, 306-316.

Tingle T. N., Hochella M. F., Becker C. H. and Malhotra R. (1990) Organic compounds on crack surfaces in olivine from San Carlos, Arizona, and Hualalai Volcano, Hawaii. *Geochim. Cosmochim. Acta* **54**, 477-485.

Tingle T. N., Mathez E. A. and Hochella M. F. (1991) Carbonaceous matter in peridotites and basalts studied by XPS, SALI, and LEED. *Geochim. Cosmochim. Acta* **55**, 1345-1352.

Wimpenny J., Gislason S. R., James R. H., Gannoun A., Pogge Von Strandmann P. A. E. and Burton K. W. (2010) The behaviour of Li and Mg isotopes during primary phase dissolution and secondary mineral formation in basalt. *Geochim. Cosmochim. Acta* **74**, 5259-5279.

Wogelius R. A. and Walther J. V. (1991) Olivine dissolution at 25 °C: effects of pH, CO_2, and organic acids. *Geochim. Cosmochim. Acta* **55**, 943-954.

Wogelius R. A. and Walther J. V. (1992) Olivine dissolution kinetics at near-surface conditions. *Chem. Geol.* **97**, 101-112.

Tables

Table 1: Techniques applied, sample type, reaction conditions and secondary product presence for all experiments (atm: atmospheric pressure; r.t.: room temperature).

Sample	Analysis techniques	Sample type	H_2O (ml)	Pressure (bar)	Tempera-ture (°C)	Oxygen presence	Reaction duration	Surface coating
Reaction in air (Section 3.2)								
Ex01	AFM	Single crystal[a]	-	atm	r.t.	Yes	< 30 mins, 4 hours	None
Ex02	XPS	Fragments[b] / powder[c]	-	atm	r.t.	Yes	< 1 mins	None
Reaction in water (Section 3.3)								
Ex03	AFM	Single crystal[a]	25	atm	r.t. .	Yes	4, 5, 10 days	None
Ex04	AFM	Fragments[b]	100	3	120	Yes	4 days	Redish
Reaction in water with increased CO_2 pressure (Section 3.4)								
Ex05	AFM	Fragments[b]	100	50	r.t.	Yes	4 days	None
Ex06	TEM, SEM, XRD, XPS	Fragments[b] / powder[c]	100	70-80	120	Yes	4 days	Red
Ex07	SEM, XPS, XRD	Fragments[b] / powder[c]	100	55-65	120	No	4 days	Bright red

[a] Freshly fractured single crystal.
[b] ~0.05 grams of fresh crystal fragments.
[c] ~0.3 grams of crushed powder with particle size ~50 μm.

Table 2. The composition (expressed as oxide weight %) for the four main phases from the peridotite specimen obtained using electron microprobe analysis. The values are averages of several measurements from various areas of the nodule. The proportion of cations is calculated on the basis of 4, 3, 6, and 4 oxygen molecules for the olivine, enstatite, diopside and spinel.

	Olivine	**Enstatite**	**Diopside**	**Spinel**
SiO_2	40.96	55.33	52.52	0.10
FeO	8.79	5.61	3.08	14.04
CaO	0.17	1.34	19.58	0.01
NiO	0.38	0.12	0.05	N/A
MgO	49.96	32.72	17.30	18.61
Al_2O_3	0.05	3.66	4.38	32.70
MnO	0.12	0.12	0.13	0.15
TiO_2	0.01	0.06	0.16	0.26
Cr_2O_3	N/A	N/A	N/A	34.29
Total	100.45	98.97	97.19	100.14
	Numbers of ions on the basis of O			
Si	0.996	0.963	1.939	0.003
Al	0.002	0.075	0.191	1.112
Cr	N/A	N/A	N/A	0.782
Fe	0.179	0.082	0.095	0.339
Mg	1.811	0.849	0.952	0.800
Ca	0.004	0.025	0.774	0.000
Ni	0.007	0.002	0.001	N/A
Mn	0.003	0.002	0.004	0.004
Ti	0.000	0.001	0.005	0.006

Olivine reactivity with CO_2 and H_2O on a microscale: Implications for carbon sequestration.

Table 3. The relative atomic concentrations obtained from XPS analyses on fresh and reacted olivine sample surfaces. Reaction time was 4 days at 120 °C and elevated CO_2 partial pressure. Depth of analysis is a few nanometers. The higher magnesium and lower carbon signals for samples that had been ground (powders) compared to crystal sample surfaces suggest the presence of original carbon compounds that coated old olivine cracks and crystal boundaries. The higher concentration of iron and oxygen on reacted surfaces indicates formation of iron oxides.

Sample ID	**Sample type**	**Mg**	**Fe**	**Si**	**O**	**Al**	**C**
	Fresh olivine						
Ex02	Crystals	7	1	15	45	8	25
	Powder	28	1	16	46	3	6
	High P-T reacted olivine						
Ex06	Crystals 1	1	10	8	54	3	24
	Crystals 2	-	-	34	54	-	12
	Powder	12	5	19	56	3	5
	Oxygen deficient high P-T reacted olivine						
Ex07	Crystals	3	14	13	60	2	8
	Powder	14	7	17	55	2	5

Figure Captions

Fig. 1. (a) Grains of the four sample constituents from left to right: forsterite, aluminium rich diopside, enstatite, and spinel that were picked from the peridotite. (b) Olivine crystals reacted in water for 4 days at 120 °C and 70 bars of total pressure. The red surface coating was clear evidence for the formation of iron oxide as a reaction product.

Fig. 2. A thin section from the peridotite nodule under crossed polarisers. The primary minerals were only weakly weathered along grain boundaries and contained generations of gaseous or liquid penetrations. Fractures, such as those indicated by the arrows, reveal old surfaces that can be coated by carbon compounds (XPS evidence, Table 3) and reaction products (Fig. 3c).

Fig. 3. AFM measurements of a freshly prepared olivine surface with (a) aligned dislocations, (b) a surface reacted with air for 4 hours, and (c) a surface that is covered by original reaction products, such as would be observed along one of the fractures such as we see in Figure 2.

Fig. 4. AFM images of olivine surfaces exposed to water for 4, 5 and 10 days. The surfaces showed indications of (a) crystal dissolution and secondary phase formation, (b) loosely bound material, and (c) bacteria.

Fig. 5. AFM image of a typical olivine surface reacted in water at room temperature and 50 bars of CO_2 for 4 days. The orientated linear features are interpreted to represent either crystals that have grown or ends of subparallel linear dislocations leached out as the olivine dissolves.

Fig. 6. TEM image of reacted powder. The black arrow shows an olivine fragment covered with secondary material.

Olivine reactivity with CO_2 and H_2O on a microscale: Implications for carbon sequestration.

Fig. 7. SEM images of olivine crystals after reaction in water for 4 days at 120 °C and total pressure at 70-80 bars. Surface character varies. (a) exfoliating flakes probably of phyllosilicate (a-c) spheres typical of amorphous silica, (b), (d) and (e) rods which presumably correspond to a network of dislocations with insoluble precipitates, inherited from the parent olivine.

Fig. 8. XRD patterns of the secondary products on the olivine surface after reaction in water for 4 days at 120 °C and total pressure of 70-80 bars (Ex06) and on the olivine surface reacted in water where oxygen has been removed, for 4 days at 120 °C with pressure at 55-65 bars (Ex07). The pattern for olivine reacted at supercritical CO_2 conditions matched hematite, magnesian calcite and magnesite. The pattern for the olivine reacted in the oxygen free solutions matched forsterite, hematite and magnesian calcite. The uneven background is caused by the glass substrate.

Fig. 9. The oxygen (1s) peaks of XPS spectra from powders, including fresh olivine (Ex02 Powder), olivine reacted under supercritical CO_2 conditions (Ex06 Powder) and oxygen free conditions (Ex07 Powder). The increase in FWHM (peak full width at half maximum) for the reacted samples indicates the formation of secondary products. The peak extension toward lower binding energy suggests the formation of iron oxides and toward higher binding energy, carbonate minerals, clays or silica.

Fig. 10. SEM images from olivine reacted under oxygen free conditions. The crystals were reacted in water for 4 days at 120 °C and 55-65 bars. (a) The reaction created etch pits and gaping cracks. (b) Networks of secondary products were sometimes observed bordering steps on the olivine surface, indicating that the crystal degenerated along preferred directions. Insert (b) is a zoom, which shows needles formed on the olivine substrate. The needles can appear as three fold twins. (c) The components released from olivine precipitate nearby as a surface network of secondary products consisting of rosette and needle shaped crystals.

Figures

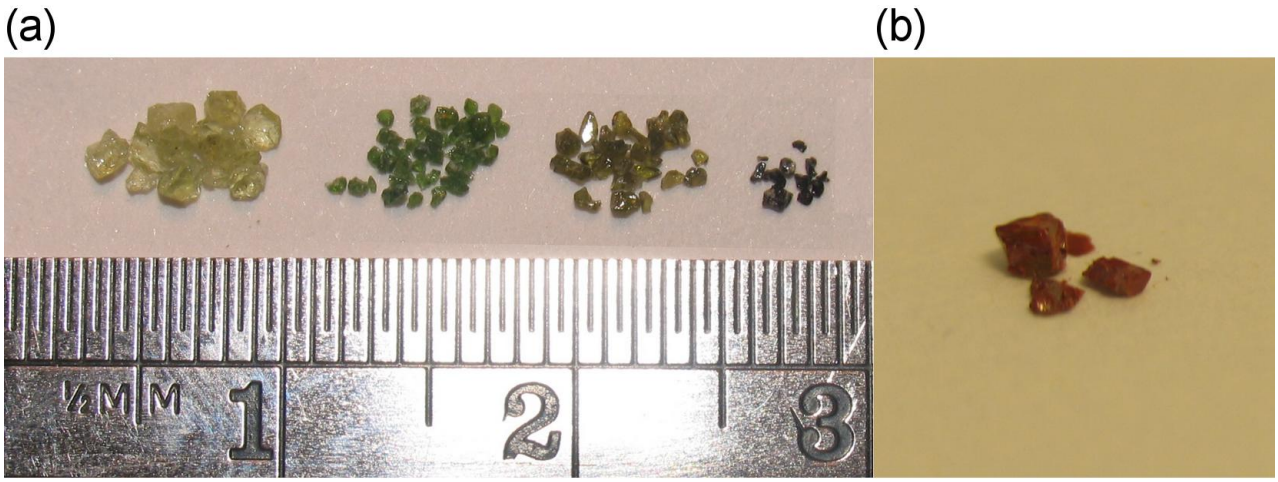

Fig. 1.

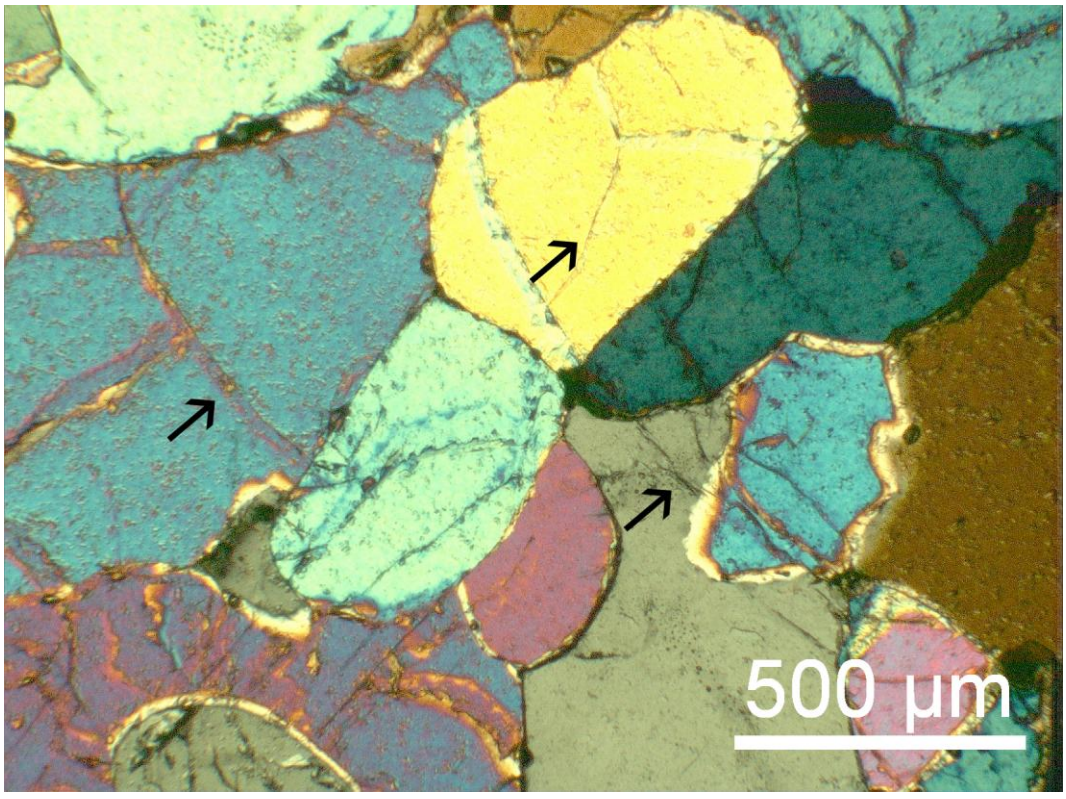

Fig. 2.

Olivine reactivity with CO_2 and H_2O on a microscale: Implications for carbon sequestration.

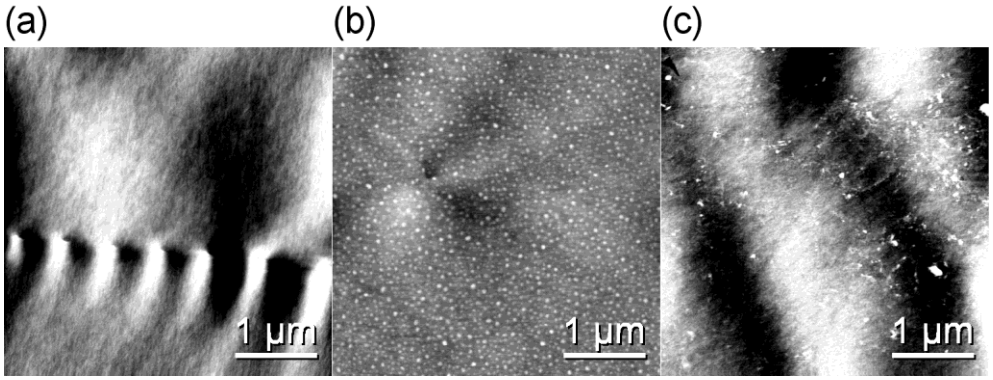

Fig. 3.

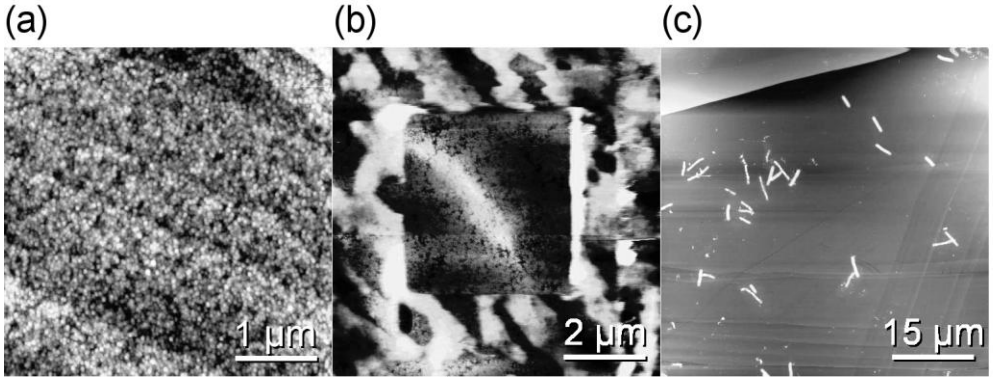

Fig. 4.

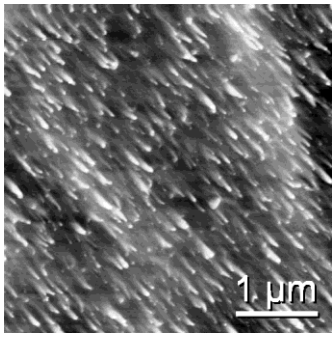

Fig. 5.

Olivine reactivity with CO_2 and H_2O on a microscale: Implications for carbon sequestration.

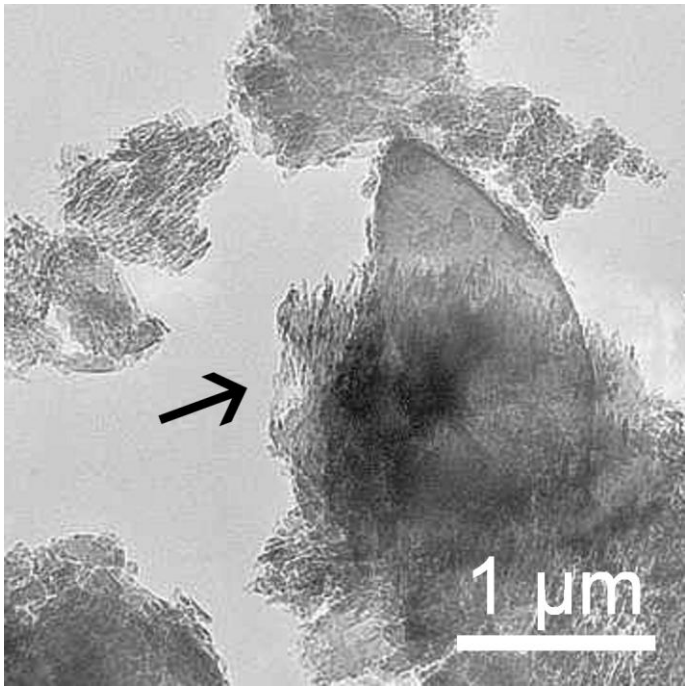

Fig. 6.

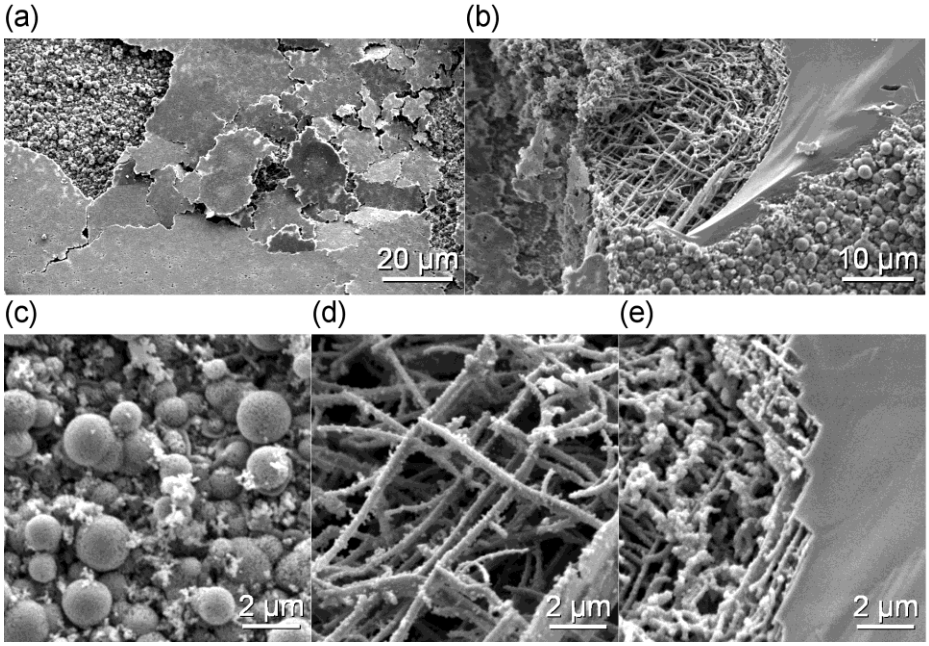

Fig. 7.

Olivine reactivity with CO_2 and H_2O on a microscale: Implications for carbon sequestration.

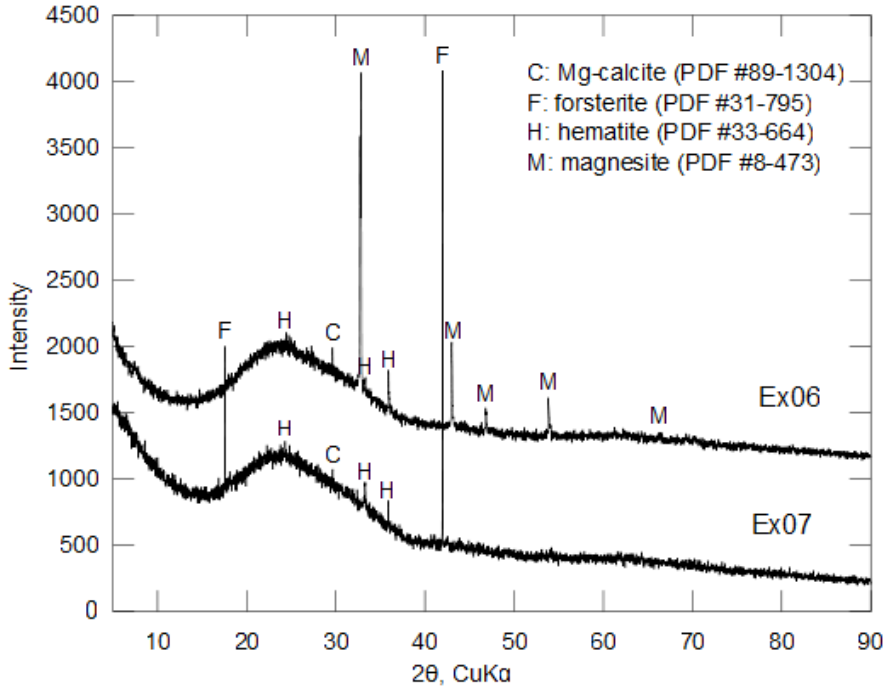

Fig. 8.

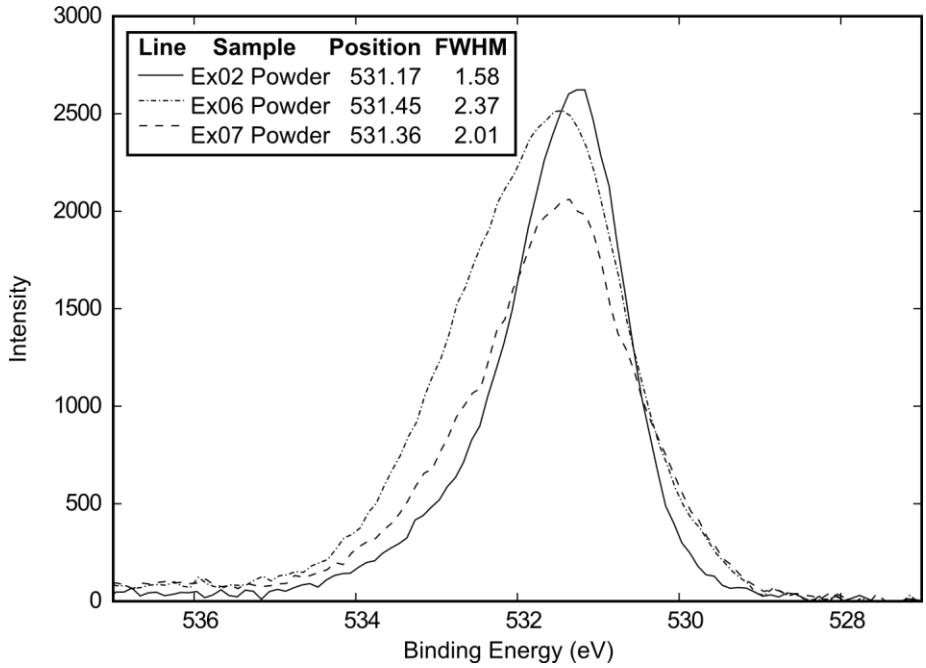

Fig. 9.

Olivine reactivity with CO_2 and H_2O on a microscale: Implications for carbon sequestration.

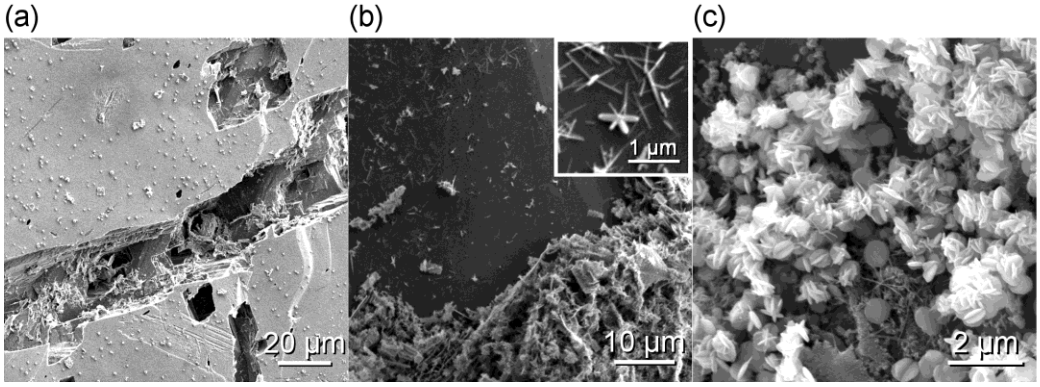

Fig. 10.

Olivine reactivity with CO_2 and H_2O on a microscale: Implications for carbon sequestration.